Towards the prediction of combustion-generated noise in non-premixed turbulent flames using large-eddy simulation

By M. Ihme, D. Bodony AND H. Pitsch

1. Motivation and objectives

Fossil fuel combustion is presently, as well as in the foreseeable future, the primary technology used to convert chemically-bound energy into electrical, mechanical, and thermal energy. Unfortunately, this process is typically accompanied by unwanted effects, such as pollutant formation and noise generation. In the design of modern combustion devices, the minimization of these effects has become a primary challenge. Numerical simulations promise to be a viable tool to address this design challenge if adequate models are available. The large-eddy simulation (LES) technique has been demonstrated to provide good accuracy in simulations of complex turbulent flow configurations. In LES, the larger, energy-containing scales are numerically resolved, and the smaller, approximately isotropic scales are unresolved and have to be modeled. LES has successfully been applied in numerical simulations of partially premixed and non-premixed open flames (Pitsch & Steiner 2000; Kempf *et al.* 2001), as well as in more complex cases such as gas turbine combustors (Kim *et al.* 1999; Moin 2002; di Mare *et al.* 2004). Especially for a highly dynamic flow configuration, an accurate prediction of the unsteady flow field appears to be of importance.

Time-accurate resolution of a wide range of turbulent eddies is of importance for the prediction of flow-induced noise, because eddies significantly contribute to noise radiation in unconfined turbulent flows such as jets and mixing layers. In recent years, hybrid methods, among others, have been used to predict the noise generated by isothermal and heated jets at subsonic and supersonic conditions (Zhao *et al.* 2001; Bodony & Lele 2005; Boersma 2005). In such methods, LES techniques for the prediction of the unsteady turbulent flow field and the acoustic source term distribution are combined with the acoustic analogy and are used to compute radiated sound perceived at a distant location.

Combustion-generated noise, however, is different from jet noise and is considerably less understood. This can be attributed to the addition of unsteady combustion and heat release to the already turbulent flow. Combustion-generated noise can be characterized either as direct or as indirect (Strahle 1975). Direct noise describes the expansion of a gas volume at constant pressure due to rapid heating. The hot gas performs work on its colder surroundings, thereby generating acoustic and non-acoustic waves. The acoustic waves propagate at the speed of sound and are perceived as noise. The responsible combustion source can be characterized as an acoustic monopole with a strength that depends on the rate of change of the reaction rate and on the reaction. Depending on the mode of combustion, the reaction rate is governed by different physical mechanisms. This suggests that the distinct combustion processes are characterized by different acoustic behavior.

Indirect combustion noise, on the other hand, is generated by the convection of large-

scale entropy non-uniformities through strong pressure gradients, but such noise is relevant only in enclosed combustors such as gas turbines. Because of the strong pressure drop across the turbine stage, it can be expected that entropy noise is the dominant source over direct combustion noise in gas turbine engines (Muthukrishnan *et al.* 1978).

The objective of the present work is the development of a numerical method for the prediction of combustion-generated noise in unconfined non-premixed jet flames using the LES technique and the acoustic theory based on Lighthill's analogy (Lighthill 1952). This method is expected to provide physical insight into the different sound-generating mechanisms in non-premixed flames while also allowing for a quantification of the importance and location of acoustic sources. In this application, combustion-generated noise is assumed to be a passive process in the sense that small acoustic pressure fluctuations have negligible effects on the acoustic source term intensity. From this perspective, combustion-generated noise is different from the thermo-acoustic instabilities that can occur in lean premixed confined combustors in which the flame is an active part of the acoustic system and acoustic fluctuations interact with unsteady heat release.

The well-characterized simple turbulent jet flame, DLR-A (Deutsches Zentrum für Luft- und Raumfahrt, German Aerospace Center), is used as a test case. Measurements of scalar species and velocity components have been taken at various locations within this flame (Bergmann *et al.* 1998; Meier *et al.* 2000; Schneider *et al.* 2003). Recently, spectral noise emissions and sound pressure levels of this flame have also been quantified (Singh *et al.* 2003, 2004).

This paper is organized as follows. The mathematical models to describe the non-premixed turbulent combustion process and the associated combustion generated noise are presented in Section 2. The nature and intensity of the different acoustic source terms appearing in the wave equation are analyzed in Section 2.3.2. The experimental conditions and the setup for the numerical simulation of the simple jet flame (DLR flame A) are described in Section 3. Simulation results are discussed and compared with experimental data in Section 4.

2. Mathematical model

In the present work, Lighthill's acoustic analogy is employed to predict the radiated sound field emitted from a non-premixed turbulent flame. In this analogy, the noise-generating sources in a limited flow domain, $\Omega_{\mathcal{F}}$, are represented by acoustically equivalent source term distributions embedded in a homogeneous stagnant fluid, $\Omega_{\mathcal{A}}$ (see Fig. 1), with constant reference properties $a_{\rm ref}, \rho_{\rm ref}$, and $p_{\rm ref}$. The exit Mach number, $\mathrm{M} = U_{\rm ref}/a_{\rm ref}$, based on the pipe bulk exit velocity and the speed of sound in air at room temperature, is very low, and compressibility effects can be neglected. Therefore, the turbulent reactive flow field and the acoustic source term distribution are computed using a low-Mach number variable density LES code. The flamelet-based, non-premixed turbulent combustion model and Lighthill's analogy are briefly presented in the following sections.

2.1. *Governing equations*

The instantaneous conservation equations for mass and momentum, evaluated in $\Omega_{\mathcal{F}}$, can be written in dimensionless form as

$$\mathcal{D}_\tau \rho = -\rho \nabla_{\boldsymbol{y}} \cdot \boldsymbol{u}\,, \tag{2.1a}$$

$$\rho \mathcal{D}_\tau \boldsymbol{u} = -\nabla_{\boldsymbol{y}} p + \frac{1}{\mathrm{Re}} \nabla_{\boldsymbol{y}} \cdot \underline{\underline{\sigma}}\,, \tag{2.1b}$$

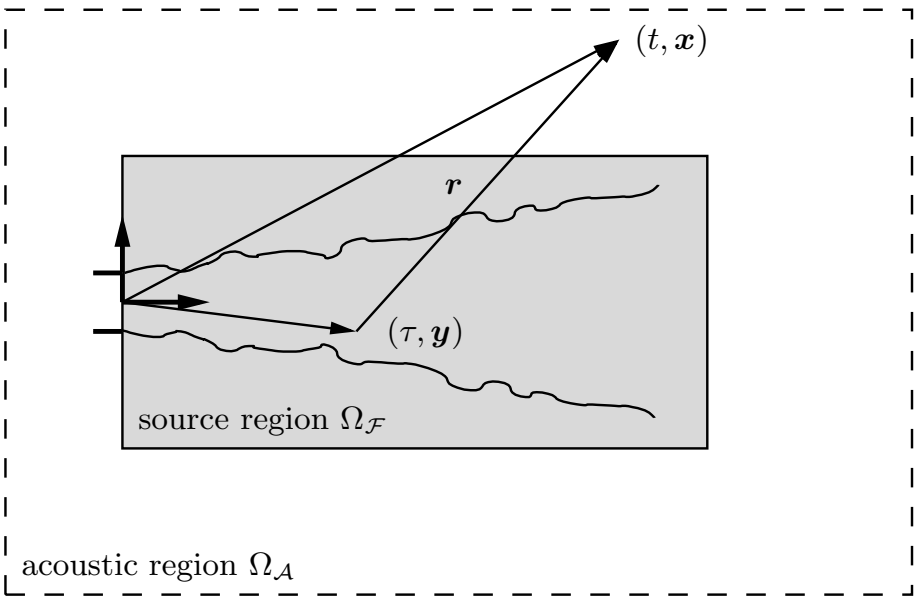

FIGURE 1. Model definition for aerodynamically generated sound; $(\tau, \boldsymbol{y})$ denotes a point in the acoustic source region $\Omega_{\mathcal{F}}$ and $(t, \boldsymbol{x})$ represents the point of perception in the acoustic domain $\Omega_{\mathcal{A}}$.

in which $\boldsymbol{u}$ is the velocity vector, p is the pressure, $\underline{\underline{\sigma}}$ represents the viscous stress tensor, and $\mathcal{D}_\tau = \partial_\tau + \boldsymbol{u}\cdot\nabla_{\boldsymbol{y}}$ is the substantial derivative. External volume forces due to buoyancy are neglected because of the small Richardson number of $\mathrm{Ri} \approx \mathcal{O}(10^{-5})$ for the present case. The following dimensionless variables are used in (2.1) and (2.8) below

$$\begin{aligned}
&\mathcal{D}_\tau = \frac{D_{\mathrm{ref}}}{U_{\mathrm{ref}}}\mathcal{D}_\tau^*\,, \quad \nabla_{\boldsymbol{y}} = D_{\mathrm{ref}}\nabla_{\boldsymbol{y}}^*\,, \quad \boldsymbol{u} = \frac{\boldsymbol{u}^*}{U_{\mathrm{ref}}}\,, \quad \rho = \frac{\rho^*}{\rho_{\mathrm{ref}}}\,,\\
&p = \frac{p^*}{\rho_{\mathrm{ref}}U_{\mathrm{ref}}^2}\,, \quad \nu = \frac{\nu^*}{\nu_{\mathrm{ref}}}\,, \quad \alpha_\psi = \frac{\alpha_\psi^*}{\alpha_{\mathrm{ref}}}\,, \quad \underline{\underline{\sigma}} = \frac{\underline{\underline{\sigma}}^* D_{\mathrm{ref}}}{\rho_{\mathrm{ref}}\nu_{\mathrm{ref}}U_{\mathrm{ref}}}\,,\\
&z = \frac{z^*}{Z_{\mathrm{ref}}}\,, \quad c = \frac{c^*}{C_{\mathrm{ref}}}\,, \quad h = \frac{h^*}{c_{\mathrm{p,ref}}\Delta\theta_{\mathrm{ref}}}\,, \quad \dot\omega_{\mathrm{c}} = \frac{\dot\omega_c^* W_{\mathrm{ref}}}{C_{\mathrm{ref}}\rho_{\mathrm{ref}}A_{\mathrm{ref}}}\exp\left\{\frac{E_{\mathrm{ref}}}{\mathcal{R}\theta_{\mathrm{ref}}}\right\}\,,\\
&\theta = \frac{\theta^* - \theta_0^*}{\Delta\theta_{\mathrm{ref}}}\,, \quad \chi_z = \frac{D_{\mathrm{ref}}^2}{\alpha_{\mathrm{ref}}}\chi_z^*\,.
\end{aligned} \tag{2.2}$$

The asterisk refers to a dimensional quantity and the subscript "ref" denotes a reference quantity in the undisturbed far field or a geometric property based on the jet fuel pipe. In particular, ν_{ref}, α_{ref}, and $c_{\mathrm{p,ref}}$ refer to properties of the fuel. Other reference quantities are based on the undisturbed reference field. The diameter of the fuel pipe and pipe bulk exit velocity are denoted by D_{ref} and U_{ref}, respectively. The kinematic viscosity is denoted by ν, α_ψ is the molecular diffusivity, $\dot\omega_c$ is the chemical production rate of the progress variable, h is the enthalpy, c_{p} is the heat capacity at constant pressure, and $\Delta\theta$ is the temperature difference. The mixture fraction and progress variable are denoted by z and c, respectively, W is the molecular weight, and A is the frequency factor. The universal gas constant is denoted by $\mathcal{R}$, and E is the activation energy. Using

this non-dimensionalization, the following similarity parameters can be formed

$$\begin{aligned}
\text{Reynolds number:} \quad & \mathrm{Re}=\frac{U_{\mathrm{ref}} D_{\mathrm{ref}}}{\nu_{\mathrm{ref}}} \,, \\
\text{Schmidt number:} \quad & \mathrm{Sc}=\frac{\nu_{\mathrm{ref}}}{\alpha_{\mathrm{ref}}} \,, \\
\text{Damköhler number:} \quad & \mathrm{Da}=\frac{D_{\mathrm{ref}}}{U_{\mathrm{ref}}} \frac{\rho_{\mathrm{ref}} A_{\mathrm{ref}}}{W_{\mathrm{ref}}} \exp\left\{-\frac{E_{\mathrm{ref}}}{\mathcal{R}\theta_{\mathrm{ref}}}\right\} \,, \\
\text{Eckert number:} \quad & \mathrm{Ec}=\frac{U_{\mathrm{ref}}^2}{c_{\mathrm{p,ref}} \Delta\theta_{\mathrm{ref}}} \,, \\
\text{Mach number:} \quad & \mathrm{M}=\frac{U_{\mathrm{ref}}}{a_{\mathrm{ref}}} \,.
\end{aligned}$$

Values of these parameters for the configuration of interest will be given in Section 3.1.

2.2. *Combustion model*

In the flamelet model (Peters 1983, 1984), a non-premixed flame is considered to be an ensemble of laminar flamelets. The steady chemical state of the flame is obtained from the solution of the steady flamelet equations,

$$-\frac{\chi_z}{2}\partial_Z^2 \boldsymbol{\psi} = \dot{\boldsymbol{\omega}} \,, \tag{2.3}$$

and is a function of the mixture fraction and scalar dissipation rate

$$\chi_z = 2\alpha_z \left|\nabla_{\boldsymbol{y}} z\right|^2 \,. \tag{2.4}$$

In (2.3), $\dot{\boldsymbol{\omega}}$ is the vector of the source terms of species and temperature, which are denoted by the vector $\boldsymbol{\psi}$. Note that the source term in the temperature equation contains an additional diffusive contribution. The solutions of (2.3) at stoichiometric condition, $z = Z_{\mathrm{st}}$, can be represented by the so-called S-shaped curve. The lower and upper branches of this curve describe the stable burning and non-reacting states, whereas the middle branch is unstable. Since multiple solutions exist for a certain range of $\chi_{z,\mathrm{st}}$, a parameterization using only z and $\chi_{z,\mathrm{st}}$ cannot represent the entire solution space.

In order to identify all flamelet solutions along the S-shaped curve, a reaction progress parameter λ is introduced in the flamelet/progress variable (FPV) model. This model has been proposed by Pierce & Moin (2004) for application in LES. The reaction progress parameter is based on a reactive scalar, the progress variable c, and is defined to be independent of the mixture fraction. Using this parameter, the state relation for all chemical and thermodynamical variables can be written as

$$\boldsymbol{\psi} = \mathcal{F}_{\boldsymbol{\psi}}(z, \lambda) \,. \tag{2.5}$$

The progress variable is a linear combination of some product mass fractions and can be obtained from (2.5) as

$$c = \mathcal{F}_c(z, \lambda) \,. \tag{2.6}$$

Assuming that a unique inversion of $\mathcal{F}_c$ exists, the reaction progress parameter in (2.5) can be eliminated by inverting the flamelet table, (2.6), and all chemical species can then be expressed in terms of z and c only:

$$\boldsymbol{\psi} = \mathcal{G}_{\boldsymbol{\psi}}(z, c) \,. \tag{2.7}$$

In addition to the solution of the Navier-Stokes equations, the FPV model requires the

solution of the following transport equations for z and c:

$$\rho\mathcal{D}_\tau z = \frac{1}{\mathrm{ReSc}}\nabla_{\boldsymbol{y}}\cdot(\rho\alpha_z\nabla_{\boldsymbol{y}} z)\ , \tag{2.8a}$$

$$\rho\mathcal{D}_\tau c = \frac{1}{\mathrm{ReSc}}\nabla_{\boldsymbol{y}}\cdot(\rho\alpha_c\nabla_{\boldsymbol{y}} c) + \mathrm{Da}\rho\dot{\omega}_c\ . \tag{2.8b}$$

The equations of motion (2.1) and the combustion model (2.8) are then coupled through the density, which is obtained from the flamelet library

$$\rho = \mathcal{G}_\rho(z, c)\ . \tag{2.9}$$

2.3. *Acoustic model*

2.3.1. *Wave equation*

In the DLR flame, sound is generated both by the turbulent flow field, primarily through unsteady Reynolds stresses, and by the combustion process in $\Omega_{\mathcal{F}}$. This sound propagates as acoustic waves to the point of perception $(t, \boldsymbol{x})$ located in the acoustic domain $\Omega_{\mathcal{A}}$ (see Fig. 1). An inhomogeneous wave equation for the pressure disturbance can be derived from the exact equations of motion by performing the operation $\partial_\tau(2.1a) - \nabla_{\boldsymbol{y}}\cdot(2.1b)$ and by then adding the term $\mathrm{M}^2\partial_\tau^2 p$ to both sides (Lighthill 1952, 1954). This leads to

$$\mathrm{M}^2\partial_\tau^2 p - \Delta_{\boldsymbol{y}} p = \nabla_{\boldsymbol{y}}\cdot\nabla_{\boldsymbol{y}}\cdot\left(\rho\boldsymbol{u}\boldsymbol{u} - \frac{1}{\mathrm{Re}}\underline{\underline{\sigma}}\right) - \partial_\tau^2(\rho - \mathrm{M}^2 p)\ . \tag{2.10}$$

The argument of the last term on the right hand side of (2.10) has been termed the "excess density" (Crighton *et al.* 1992), $\rho_{\mathrm{e}} = (\rho - 1 - \mathrm{M}^2(p - p_{\mathrm{ref}}))$. Large spatial and temporal variations of entropy occur due to rapid heat release in chemical reacting flows, and hence, this term becomes an important source in combustion-generated sound. The time derivative of ρ_{e} can be written as (Crighton *et al.* 1992)

$$\partial_\tau\rho_{\mathrm{e}} = \frac{1}{\rho}\mathcal{D}_\tau\rho + \nabla_{\boldsymbol{y}}\cdot((1-\rho)\boldsymbol{u}) - \mathrm{M}^2\partial_\tau(p - p_{\mathrm{ref}})\ . \tag{2.11}$$

Using (2.9), the substantial derivative of the density can be written as

$$\mathcal{D}_\tau\rho = \partial_Z\mathcal{G}_\rho\mathcal{D}_\tau z + \partial_C\mathcal{G}_\rho\mathcal{D}_\tau c \tag{2.12}$$

and the wave equation can be reformulated as

$$\begin{aligned}\mathrm{M}^2\partial_\tau^2 p - \Delta_{\boldsymbol{y}} p = \gamma \equiv{}& \nabla_{\boldsymbol{y}}\cdot\nabla_{\boldsymbol{y}}\cdot\underbrace{(\rho\boldsymbol{u}\boldsymbol{u})}_{\underline{\underline{T}}_{\mathrm{R}}} - \partial_\tau\nabla_{\boldsymbol{y}}\cdot\underbrace{((1-\rho)\boldsymbol{u})}_{\boldsymbol{F}_{\mathrm{M}}} - \mathrm{Da}\partial_\tau\underbrace{\left(\frac{1}{\rho}\partial_C\mathcal{G}_\rho\dot{\omega}_c\right)}_{Q_{\mathrm{H}}} \\ & - \frac{1}{\mathrm{ReSc}}\partial_\tau\underbrace{\left(\frac{1}{\rho^2}\left\{\partial_Z\mathcal{G}_\rho\nabla_{\boldsymbol{y}}\cdot(\rho\alpha_z\nabla_{\boldsymbol{y}} z) + \partial_C\mathcal{G}_\rho\nabla_{\boldsymbol{y}}\cdot(\rho\alpha_c\nabla_{\boldsymbol{y}} c)\right\}\right)}_{Q_{\mathrm{D}}} \\ & + \mathrm{M}^2\partial_\tau^2\underbrace{(p - p_{\mathrm{ref}})}_{Q_{\mathrm{P}}} - \frac{1}{\mathrm{Re}}\nabla_{\boldsymbol{y}}\cdot\nabla_{\boldsymbol{y}}\cdot\underbrace{\underline{\underline{\sigma}}}_{\underline{\underline{T}}_{\mathrm{V}}}\ .\end{aligned} \tag{2.13}$$

Here, the terms $\underline{\underline{T}}_{\mathrm{R}}$ and $\underline{\underline{T}}_{\mathrm{V}}$ represent quadrupole sources due to unsteady Reynolds and viscous stresses. The term $\boldsymbol{F}_{\mathrm{M}}$ is a fluctuating momentum flux of dipole nature, and Q_{H},

$Q_{\rm D}$, and $Q_{\rm P}$ are monopole sources due to unsteady reaction rates, diffusion fluctuations, and pressure fluctuations, respectively.

Using a free-space Green's function, a formal solution of (2.13) can be written as

$$p'(t,\boldsymbol{x}) = (p(t,\boldsymbol{x}) - p_{\rm ref}) = \frac{1}{4\pi}\iiint_{\Omega_{\mathcal{F}}} \frac{\gamma(t-{\rm M}|\boldsymbol{x}-\boldsymbol{y}|,\boldsymbol{y})}{|\boldsymbol{x}-\boldsymbol{y}|}{\rm d}\boldsymbol{y}\ . \tag{2.14}$$

2.3.2. *Far field approximation and acoustic power*

The magnitude of the source terms in (2.14) at a far field location $\boldsymbol{x}$ and for an acoustically compact source can be estimated as a function of the non-dimensional parameters using the far field approximation and reciprocity relation. Then (2.14) can be written as

$$\begin{aligned} p'(t,\boldsymbol{x}) = \frac{1}{4\pi|\boldsymbol{x}|}\iiint_{\Omega_{\mathcal{F}}} & -{\rm Da}\partial_t[Q_{\rm H}]_{\mathcal{R}} + {\rm M}\frac{\boldsymbol{x}}{|\boldsymbol{x}|}\partial_t^2[\boldsymbol{F}_{\rm M}]_{\mathcal{R}} + {\rm M}^2\frac{\boldsymbol{x}\boldsymbol{x}}{|\boldsymbol{x}|^2}\partial_t^2[\underline{\underline{T}}_{\rm R}]_{\mathcal{R}} \\ & + {\rm M}^2\partial_t^2[Q_{\rm P}]_{\mathcal{R}} - \frac{{\rm M}^2}{\rm Re}\frac{\boldsymbol{x}\boldsymbol{x}}{|\boldsymbol{x}|^2}\partial_t^2[\underline{\underline{T}}_{\rm V}]_{\mathcal{R}} - \frac{1}{\rm ReSc}\partial_t[Q_{\rm D}]_{\mathcal{R}}{\rm d}\boldsymbol{y}\ , \end{aligned} \tag{2.15}$$

in which the square bracket $[\psi]_{\mathcal{R}}$ denotes $\psi(\boldsymbol{y}, t-{\rm M}|\boldsymbol{x}-\boldsymbol{y}|)$. Equation (2.15) shows that the monopole describing the unsteady reaction rate is independent of the Mach number. The dipole term scales with the Mach number and the terms containing $\underline{\underline{T}}_{\rm R}$, $\underline{\underline{T}}_{\rm V}$, and $Q_{\rm P}$ scale with ${\rm M}^2$. For low Mach number combustion, the quadrupole terms due to fluctuating viscous and Reynolds stresses are expected to be negligible, as compared with the monopole source due to unsteady heat release. It is interesting to note that the term $\underline{\underline{T}}_{\rm R}$, which is small for the present case, is the dominant source of sound in turbulent isothermal jets.

The total acoustic power $P_{\rm ac}$ of a turbulent jet with heat release can be estimated as

$$P_{\rm ac} \sim {\rm M}\,\overline{p'^2}\ , \tag{2.16}$$

and the rate at which chemical and kinetic energy is supplied to the jet can be computed from

$$\dot{E}_{\rm in} = \dot{m}\left\{h + {\rm Ec}\left(\frac{p}{\rho} + \frac{1}{2}u^2\right)\right\}\ . \tag{2.17}$$

In the case of turbulent flames, the thermal energy is usually dominant over the kinetic energy supply. With the above scaling relations and (2.15), the following observations can be made. The ratio of the acoustic power output generated by the unsteady heat release and $\dot{E}_{\rm in}$ is

$$\frac{P_{\rm ac}(Q_{\rm H})}{\dot{E}_{\rm in}} \sim {\rm M}\,{\rm Da}^2\ , \tag{2.18}$$

which scales linearly with the Mach number and quadratically with the Damköhler number. The contribution of $\boldsymbol{F}_{\rm M}$ to the acoustic power, normalized by $\dot{E}_{\rm in}$, is

$$\frac{P_{\rm ac}(\boldsymbol{F}_{\rm M})}{\dot{E}_{\rm in}} \sim {\rm M}^3\ , \tag{2.19}$$

which scales with the third power of the Mach number. Furthermore, Lighthill's well-known ${\rm M}^5$-scaling relation for the acoustic power radiated due to the unsteady Reynolds stress can be written as

$$\frac{P_{\rm ac}(\underline{\underline{T}}_{\rm R})}{\dot{E}_{\rm in}} \sim {\rm M}^5\ . \tag{2.20}$$

In the limit of large Reynolds number flows, the source term contributions due to the viscous stresses and species diffusion can be neglected, and the simplified acoustic source term can then be written as

$$\gamma_{\mathrm{a}} = \nabla_{\boldsymbol{y}} \cdot \nabla_{\boldsymbol{y}} \cdot \underline{\underline{T}}_{\mathrm{R}} - \partial_\tau \nabla_{\boldsymbol{y}} \cdot \boldsymbol{F}_{\mathrm{M}} - \mathrm{Da}\partial_\tau Q_{\mathrm{H}} + \mathrm{M}^2 \partial_\tau^2 Q_{\mathrm{P}} \; . \tag{2.21}$$

2.3.3. *Numerical implementation*

The sound field at the observer location $(t, \boldsymbol{x})$ is computed from (2.14) with the simplified source term shown in (2.21). Rather than determining the time-dependent pressure fluctuation at this location, it is usually of more interest to analyze the power spectral density $S(\omega)$ and sound pressure level (SPL) as a function of frequency ω. Introducing the forward and inverse Fourier transformations

$$\widehat{\psi}(\omega) = \int_{-\infty}^{\infty} \psi(t) \exp\left\{-\mathrm{i}\omega t\right\} \mathrm{d}t \; , \tag{2.22a}$$

$$\psi(t) = \frac{1}{2\pi} \int_{-\infty}^{\infty} \widehat{\psi}(\omega) \exp\left\{\mathrm{i}\omega t\right\} \mathrm{d}\omega \; , \tag{2.22b}$$

the Fourier transformed integral equation for the far field pressure can be written as

$$\widehat{p'}(\omega, \boldsymbol{x}) = \frac{1}{4\pi} \iiint_{\Omega_{\mathcal{F}}} \frac{\exp\left\{-\mathrm{i}\omega \mathrm{M}|\boldsymbol{x} - \boldsymbol{y}|\right\}}{|\boldsymbol{x} - \boldsymbol{y}|} \widehat{\gamma}_{\mathrm{a}}(\omega, \boldsymbol{y}) \mathrm{d}\boldsymbol{y} \tag{2.23}$$

with

$$\widehat{\gamma}_{\mathrm{a}} = \nabla_{\boldsymbol{y}} \cdot \nabla_{\boldsymbol{y}} \cdot \underline{\underline{\widehat{T}}}_{\mathrm{R}} - \mathrm{i}\omega \nabla_{\boldsymbol{y}} \cdot \widehat{\boldsymbol{F}}_{\mathrm{M}} - \mathrm{i}\omega \mathrm{Da} \widehat{Q}_{\mathrm{H}} - \mathrm{M}^2 \omega^2 \widehat{Q}_{\mathrm{P}} \; . \tag{2.24}$$

The spatial derivatives in (2.24) can be transfered to the pre-exponential term using integration by parts, giving

$$\widehat{p'}(\omega, \boldsymbol{x}) = \frac{1}{4\pi} \iiint_{\Omega_{\mathcal{F}}} \left(\underline{\underline{\kappa}} : \underline{\underline{\widehat{T}}}_{\mathrm{R}} + \boldsymbol{\lambda} \cdot \widehat{\boldsymbol{F}}_{\mathrm{M}} - \mu \left(\mathrm{Da} \widehat{Q}_{\mathrm{H}} - \mathrm{i}\omega \mathrm{M}^2 \widehat{Q}_{\mathrm{P}} \right) \right) \mathrm{d}\boldsymbol{y} \tag{2.25}$$

with

$$\kappa_{ij} = \left\{ \frac{R_i R_j}{R^3} \left(\frac{3}{R^2} + \frac{\mathrm{i}3\omega \mathrm{M}}{R} - \omega^2 \mathrm{M}^2 \right) - \frac{\delta_{ij}}{R^3} \left(1 + \mathrm{i}\omega \mathrm{M} R\right) \right\} \exp\{-\mathrm{i}\omega \mathrm{M} R\} \; , \tag{2.26a}$$

$$\lambda_i = \mathrm{i}\omega \frac{R_i}{R^3} \left(1 + \mathrm{i}\omega \mathrm{M} R\right) \exp\{-\mathrm{i}\omega \mathrm{M} R\} \; , \tag{2.26b}$$

$$\mu = \mathrm{i}\omega \frac{1}{R} \exp\{-\mathrm{i}\omega \mathrm{M} R\} \; , \tag{2.26c}$$

where Cartesian index notation has been used and $R_i = x_i - y_i$ so that $R = |\boldsymbol{x} - \boldsymbol{y}|$.

3. Numerical simulation

3.1. *Experimental conditions*

The FPV model is applied in a large-eddy simulation of a turbulent jet flame configuration (DLR flame A). This N_2-diluted CH_4-H_2/air flame has been experimentally studied by Bergmann *et al.* (1998) and by Meier *et al.* (2000). The burner configuration for the non-premixed flame consists of a central fuel nozzle of diameter D_{ref} surrounded by a co-flow nozzle of square shape. The fuel bulk velocity is U_{ref}. Co-flow air is supplied at an axial velocity of $7.11 \times 10^{-3} U_{\mathrm{ref}}$. All parameters used in the calculation are given in Tab. 1.

Parameter	Value	Units
D_{ref}	8×10^{-3}	m
U_{ref}	42.2	m/s
a_{ref}	344.33	m/s
ρ_{ref} (air)	1.169	kg/m^3
ν_{ref} (fuel)	2.2908×10^{-5}	m^2/s
α_{ref} (fuel)	4.7096×10^{-5}	m^2/s
$c_{\mathrm{p,ref}}$ (fuel)	1,815.73	J/(kg K)

Parameter	Value	Units
θ_{ref}	2,110	K
$\Delta\theta_{\mathrm{ref}}$	1,817	K
E_{ref}	1.435×10^4	J/mol
A_{ref}	216	m^3/(mol s)
W_{ref} (air)	2.877×10^{-2}	kg/mol
C_{ref}	1.0	-
Z_{ref}	1.0	-

TABLE 1. Reference parameters for the simulation.

The jet fluid consists of a mixture of 22.1 % methane, 33.2 % hydrogen and 44.7 % nitrogen by volume with a stoichiometric mixture fraction of $Z_{\mathrm{st}} = 0.167$. It has been reported that the DLR flame A burns very stably and that lift-off is not observed (Meier *et al.* 2000).

The Reynolds number, which is based on the nozzle diameter, the pipe bulk exit velocity and the kinematic viscosity of the fuel mixture, is 14,740. The Schmidt number is $\mathrm{Sc} = 0.486$, the Mach number is $\mathrm{M} = 0.123$, and the Eckert number is $\mathrm{Ec} = 5.4 \times 10^{-4}$. The Damköhler number is the ratio of the characteristic flow time scale to the chemical time scale. To compute this ratio, an appropriate chemical time scale must be determined. Here, this time scale comes from writing the definition of the progress variable $c = y_{\mathrm{CO_2}} + y_{\mathrm{CO}} + y_{\mathrm{H_2O}} + y_{\mathrm{H_2}}$. The largest contribution to c comes from the mass fraction of water. A sensitivity analysis has been performed which shows that water is primarily formed by the fast shuffle reaction

$$\mathrm{OH} + \mathrm{H_2} \rightleftharpoons \mathrm{H_2O} + \mathrm{H}\,. \tag{3.1}$$

Therefore, the chemical time scale appearing in the Damköhler number is determined using the frequency factor and activation energy of (3.1). Performing this calculation gives $\mathrm{Da} = 0.734$.

3.2. *Numerical setup and large-eddy simulation*

The Favre-filtered conservation equations for mass, momentum, mixture fraction and progress variable are solved in a cylindrical coordinate system $\boldsymbol{y} = (y, r, \varphi)^{\mathsf{T}}$ in $\Omega_{\mathcal{F}}$. A Favre-filtered quantity is defined as

$$\widetilde{\psi}(\tau, \boldsymbol{y}) = \frac{1}{\overline{\rho}(\tau, \boldsymbol{y})} \int \rho(\tau, \boldsymbol{y}')\psi(\tau, \boldsymbol{y}')G(\tau, \boldsymbol{y} - \boldsymbol{y}')\mathrm{d}\boldsymbol{y}'\,, \tag{3.2}$$

where G is the LES filter kernel and the residual field is $\psi'' = \psi - \widetilde{\psi}$. The residual stresses and scalar fluxes that appear in the transport equations after filtering are modeled by a dynamic procedure (Pierce & Moin 2004), and the filtered chemical source term is closed using a presumed joint PDF.

Only the upper, stable burning branch of the S-shaped curve is used to parameterize the flamelet library $\mathcal{G}(z, c)$. This essentially reduces the FPV model to the classical steady flamelet model, in which all chemical species are parameterized by the mixture fraction and by the scalar dissipation rate. This choice was motivated by the observation that the

simulated flame lifts off of the nozzle and subsequently extinguishes when the complete S-shaped curve is used for parameterization. Physically, this occurs because the flame is not stabilized by a pilot, and the scalar dissipation rate close to the nozzle is too high for stable burning. It can be expected that an unsteady flamelet model, as proposed by Pitsch & Ihme (2005), would lead to more physically realistic behavior close to the nozzle. As shown in Section 4, however, this simplified model leads to excellent results for the flow field and chemical species distribution, and it is likely that the unsteady FPV model would only describe the stabilization of the flame more accurately.

The geometry has been non-dimensionalized by the jet nozzle diameter D_{ref}, and the computational domain is $50 \times 20 \times 2\pi$ in axial, radial, and circumferential directions, respectively. The radial direction is discretized by 160 unevenly spaced grid points concentrated in the fuel nozzle. Fifty grid points are used to discretize the jet radius. The grid in axial direction uses 256 points and is, beginning at the nozzle exit, stretched downstream. For the discretization of the fuel pipe, which is of length $2D_{\mathrm{ref}}$, 32 equidistant grid points are used which corresponds to $\Delta y^+ \approx 50$. The grid spacing at the wall within the fuel pipe is $\Delta r^+ \approx 1.5$. The circumferential direction is equally spaced and uses 64 points. The total number of grid points used for the simulation is approximately 2.6 million. The non-dimensional minimum and maximum filter widths in the domain are $\Delta_{\min} = 1.74 \times 10^{-2}$ (boundary layer in the fuel pipe) and $\Delta_{\max} = 0.99$ (outermost grid cell at the outflow plane).

The turbulent inlet velocity profile is generated by separately performing a periodic pipe flow simulation, enforcing an empirical turbulent mean profile for the axial velocity of the form $\langle\widetilde{u}\rangle(r) = U_C(1-2r)^{1/n}$, where $n = 6.501$ (Nikuradse 1932) and where U_C is computed from the normalization condition $\int_0^{1/2} \langle\widetilde{u}\rangle r\mathrm{d}r = 1/8$. Convective outflow conditions are used at the outlet, and slip-free boundary conditions are employed at the radial boundaries.

The numerical simulation is run over ten flow-through-times to obtain a statistically stationary flow field, and statistics are collected thereafter over five flow-through-times.

4. Results and discussion

In this section, results of the large-eddy simulation are presented and compared to experimental data. Temporally and azimuthally averaged quantities are denoted by $\langle\widetilde{\psi}\rangle$ with

$$\langle\widetilde{\psi}\rangle(y,r) = \frac{1}{2\pi T}\int_{\tau}^{\tau+T}\int_{0}^{2\pi}\widetilde{\psi}(\tau,y,r,\varphi)\mathrm{d}\varphi\mathrm{d}\tau\ , \tag{4.1}$$

and the resolved averaged variance $\langle\widetilde{\psi}''^2_{<}\rangle$ is computed from

$$\langle\widetilde{\psi}''^2_{<}\rangle(y,r) = \frac{1}{2\pi T}\int_{\tau}^{\tau+T}\int_{0}^{2\pi}\Big(\widetilde{\psi}(\tau,y,r,\varphi) - \langle\widetilde{\psi}\rangle(y,r)\Big)^2\,\mathrm{d}\varphi\mathrm{d}\tau\ . \tag{4.2}$$

4.1. *Flow field and flame structure*

Axial profiles of mean and resolved root-mean square (rms) values for axial velocity, mixture fraction and temperature are compared with experimental data in Fig. 2. Numerical results are shown as solid lines, while experimental data and their estimated uncertainties are denoted by symbols. The predicted mean and rms velocity profiles obtained from

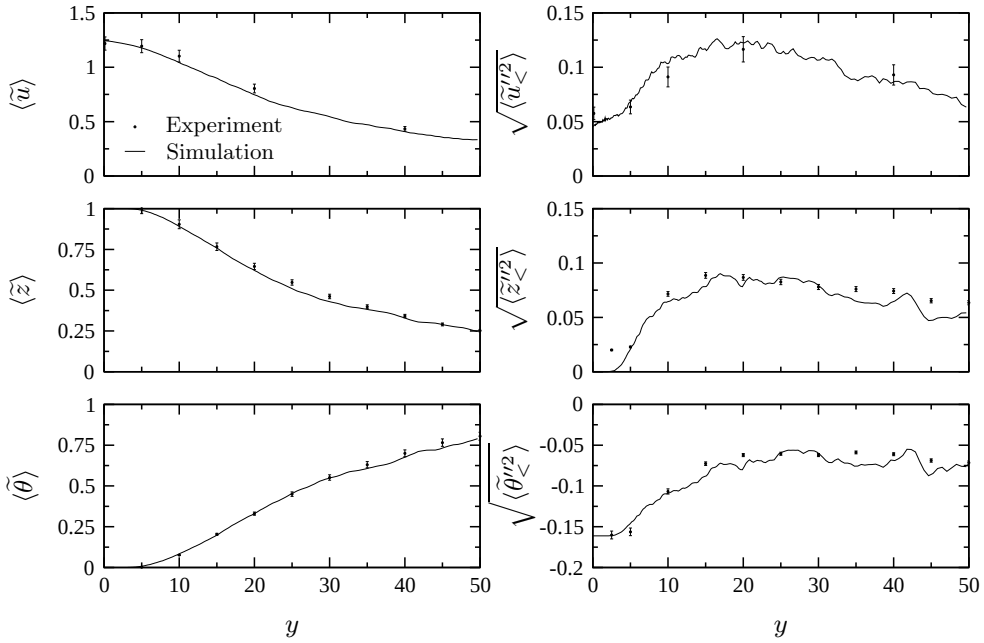

FIGURE 2. Comparison of measured (symbols) and calculated (solid lines) mean and resolved rms statistics of axial velocity, mixture fraction, and temperature along the centerline. Experimental data are plotted with estimated uncertainties.

the simulation are in good agreement with experimental data. The second row in Fig. 2 shows a comparison of the measured and predicted mean and rms mixture fraction. The stoichiometric mixture fraction is $Z_{\rm st} = 0.167$, and the stoichiometric flame length is experimentally determined to be $L_{\rm st} \approx 64.3$. Because of numerical resolution requirements the computational domain does not extend this far. However, the domain is sufficiently large to capture the turbulence-chemistry interaction that is responsible for heat release and for unsteady acoustic source term distributions. The mean mixture fraction profile is in overall good agreement with the experimental data, but a small over-prediction of the mixture fraction decay rate in the range of $20 \leq y \leq 35$ is observable. Because of the small changes in temperature with respect to mixture fraction in the rich part of the flame, this under-prediction of mixture fraction is not reflected by an over-prediction of the temperature, shown in the last row of Fig. 2. The mean temperature along the centerline is in good agreement with the experimental data.

4.2. *Combustion model*

Turbulent non-premixed combustion is strongly affected by the interaction of turbulent mixing on the small scales, diffusion between fuel and oxidizer, and chemical reactions. For an assessment of only the combustion model, it is essential to perform a flow-field independent comparison of the chemical species and temperature with experimental data. In the following, this is done by analyzing mixture fraction-conditioned data with experimental results in Fig. 3.

The mean temperature and major species, conditioned on mixture fraction and evaluated at four different axial planes, are shown in Fig. 3. The conditional temperature,

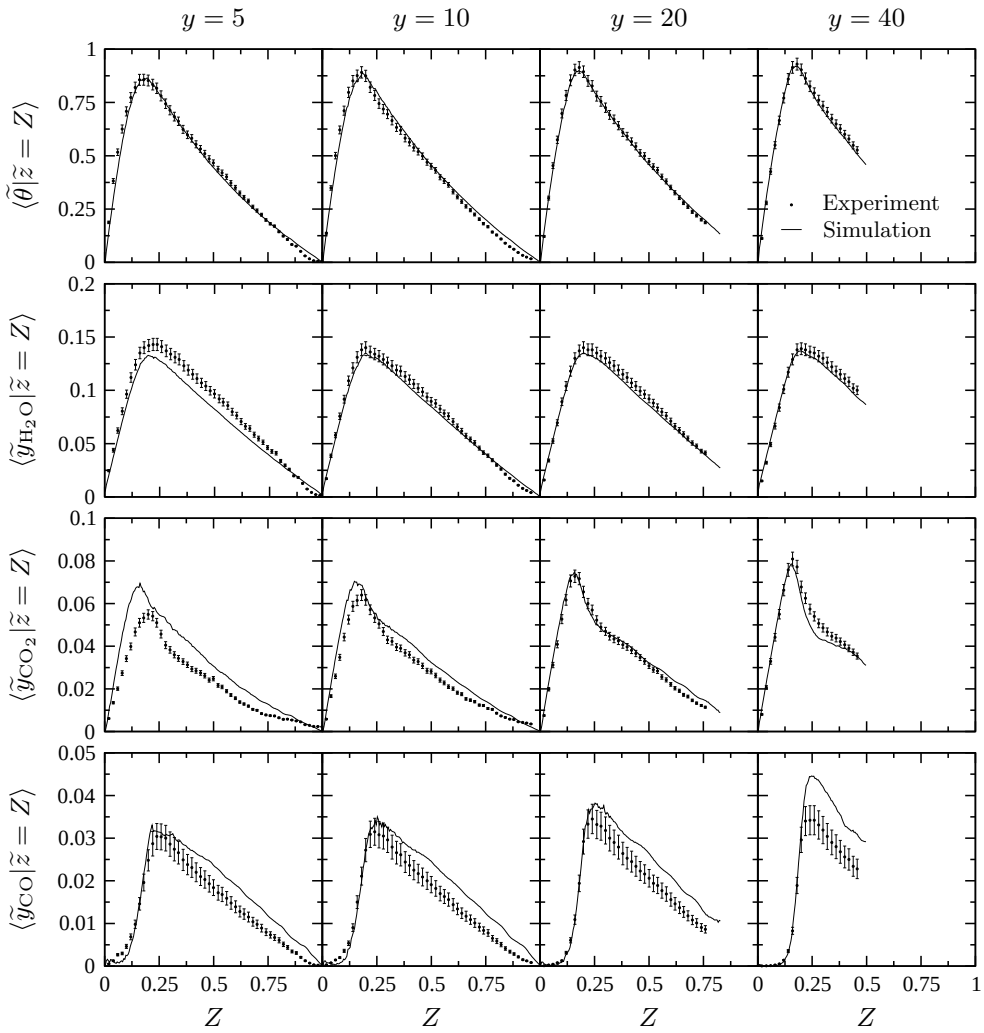

FIGURE 3. Comparison of measured (symbols) and calculated (solid lines) conditional mean mass fractions of major species and temperature at $y = 5.0, 10, 20$ and 40. Experimental data are plotted with estimated uncertainties.

shown in the first row of Fig. 3, is in good agreement with experimental data at all measurement stations. Apart from the under-prediction of the water mass fraction at $y = 5$, H_2O is also in good agreement with experimental data. Carbon dioxide and carbon monoxide agree reasonably well.

5. Conclusions and future work

In this paper, a large-eddy simulation of a N_2-diluted CH_4-H_2/air flame has been performed. Results obtained from this numerical simulation have been presented and compared with experimental data. A low Mach number, variable density LES solver was used to simulate the flame, and the FPV model was employed to describe combustion.

Results for the centerline decay of the mean velocity, mixture fraction, and temperature are in good agreement with experimental data. The analysis of the combustion model shows good agreement with measurements. Further improvements of the results close to the fuel nozzle would be expected if an appropriate model accounting for differential diffusion was used.

A model equation for the prediction of the acoustic pressure fluctuation, perceived at a far field location, is presented. This model is based on Lighthill's acoustic analogy and employs the FPV assumption in order to express the deviation from the isotropic behavior in terms of mixture fraction and progress variable. The acoustic wave equation has been analyzed in terms of the source term intensities. Four main sources have been identified as major contributors to the acoustic far field pressure.

The accurate numerical simulation of the turbulent flow field and the underlying combustion processes are necessary for the prediction of the radiated sound field, which is sensitive to the source term distribution and intensity. This exact numerical prediction of the flow field and chemical species distribution constitutes the foundation for future work which will include the prediction of the acoustic far field pressure and the analysis of the different acoustic source terms.

Acknowledgments

The authors gratefully acknowledge funding by the United States Department of Energy within the Advanced Simulation and Computing (ASC) program. We would like to thank Ed Knudsen for helpful comments on the manuscript.

REFERENCES

Bergmann, V., Meier, W., Wolff, D. & Stricker, W. 1998 Application of spontaneous Raman and Rayleigh scattering and 2D LIF for the characterization of a turbulent $CH_4/H_2/N_2$ jet diffusion flame. *Appl. Phys. B* **66**, 489–502.

Bodony, D. & Lele, S. 2005 On using large-eddy simulation for the prediction of noise from cold and heated turbulent jets. *Phys. Fluids* **17**, 085103.

Boersma, B. 2005 Large eddy simulation of the sound field of a round turbulent jet. *Theor. Comp. Fluid Dyn.* **19**, 161–170.

Crighton, D., Dowling, A., Ffowcs Williams, J., Heckl, M. & Leppington, F. 1992 *Modern Methods in Analytical Acoustics*. Springer-Verlag.

Kempf, A., Flemming, F. & Janicka, J. 2001 Large eddy simulation of a highly turbulent methane flame: application to the DLR standard flame. In *2nd Int. Symp. Turbulent Shear Flow Phenomena*, 315–320.

Kim, W., Menon, S. & Mongia, H. 1999 Large-eddy simulation of a gas turbine combustor flow. *Combust. Sci. Tech.* **143**, 25–62.

Lighthill, M. J. 1952 On sound generated aerodynamically: I: General theory. *Proc. Roy. Soc. London (A)* **211**, 564–587.

Lighthill, M. J. 1954 On sound generated aerodynamically: II: Turbulence as a source of sound. *Proc. Roy. Soc. London (A)* **222**, 1–32.

di Mare, F., Jones, W. & Menzies, K. 2004 Large eddy simulation of a model gas turbine combustor. *Combust. Flame* **137**, 278–294.

Meier, W., Barlow, R., Chen, Y. & Chen, J. 2000 Raman/Rayleigh/LIF measure-

ments in a turbulent $CH_4/H_2/N_2$ jet diffusion flame: Experimental techniques and turbulence-chemistry interaction. *Combust. Flame* **123**, 326–343.

Moin, P. 2002 Advances in large eddy simulation methodology for complex flows. *Int. J. Heat Fluid Flow* **25**, 710–720.

Muthukrishnan, M., Strahle, W. & Neale, D. 1978 Separation of hydrodynamic, entropy, and combustion noise in a gas turbine combustor. *AIAA J.* **16**, 320–327.

Nikuradse, J. 1932 Gesetzmäßigkeiten der turbulenten Strömung in glatten Rohren. *VDI Forschungsheft* .

Peters, N. 1983 Local quenching due to flame stretch and non-premixed turbulent combustion. *Combust. Sci. Tech.* **30**, 1–17.

Peters, N. 1984 Laminar diffusion flamelet models in non-premixed turbulent combustion. *Prog. Energy Combust. Sci.* **10**, 319–339.

Pierce, C. & Moin, P. 2004 Progress-variable approach for large-eddy simulation of non-premixed turbulent combustion. *J. Fluid Mech.* **504**, 73–97.

Pitsch, H. & Ihme, M. 2005 An unsteady/flamelet progress variable method for LES of nonpremixed turbulent combustion. *AIAA-2005-557*.

Pitsch, H. & Steiner, H. 2000 Large-eddy simulation of a turbulent piloted methane/air diffusion flame (Sandia flame D). *Phys. Fluids* **12**, 2541–2554.

Schneider, C., Dreizler, A., Janicka, J. & Hassel, E. 2003 Flow field measurements of stable and locally extinguishing hydrocarbon-fuelled jet flames. *Combust. Flame* **135**, 185–190.

Singh, K. K., Frankel, S. H. & Gore, J. P. 2003 Effects of combustion on the sound pressure generated by circular jet flows. *AIAA J.* **41**, 319–321.

Singh, K. K., Frankel, S. H. & Gore, J. P. 2004 Study of spectral noise emissions from standard turbulent nonpremixed flames. *AIAA J.* **42**, 931–936.

Strahle, W. C. 1975 A review of combustion generated noise. *Prog. Astro. Aero.* **37**, 229–248.

Zhao, W., Frankel, S. & Mongeau, L. 2001 Large eddy simulations of sound radiation from subsonic turbulent jets. *AIAA J.* **39**, 1469–1477.